

Impact of Current Collecting Grids on the Scalability of 3-Terminal Perovskite/Silicon Tandems with Bipolar Transistor Architecture

*Original*

Impact of Current Collecting Grids on the Scalability of 3-Terminal Perovskite/Silicon Tandems with Bipolar Transistor Architecture / Giliberti, Gemma; Cappelluti, Federica. - ELETTRONICO. - (2023), pp. 1-3. (Intervento presentato al convegno IEEE 50th Photovoltaic Specialists Conference (PVSC) tenutosi a San Juan, PR, USA nel 11-16 June 2023) [10.1109/PVSC48320.2023.10360071].

*Availability:*

This version is available at: 11583/2985153 since: 2024-01-16T13:27:44Z

*Publisher:*

IEEE

*Published*

DOI:10.1109/PVSC48320.2023.10360071

*Terms of use:*

This article is made available under terms and conditions as specified in the corresponding bibliographic description in the repository

*Publisher copyright*

IEEE postprint/Author's Accepted Manuscript

©2023 IEEE. Personal use of this material is permitted. Permission from IEEE must be obtained for all other uses, in any current or future media, including reprinting/republishing this material for advertising or promotional purposes, creating new collecting works, for resale or lists, or reuse of any copyrighted component of this work in other works.

(Article begins on next page)

# Impact of current collecting grids on the scalability of 3-terminal perovskite/silicon tandems with bipolar transistor architecture

Gemma Giliberti<sup>1\*</sup>, Federica Cappelluti<sup>1\*</sup>, *Senior Member, IEEE*

Department of Electronics and Telecommunications, Politecnico di Torino, Corso Duca degli Abruzzi 24, 10129 Torino, Italy

**Abstract**—The heterojunction bipolar transistor (HBT) structure is an attractive solution for developing three-terminal perovskite/silicon tandem solar cells compatible with dominant silicon photovoltaic devices, such as PERC and heterojunction. However, in contrast to three-terminal tandems based on interdigitated back contact silicon cells, the three-terminal HBT requires the implementation of the third contact at the base (middle) layer. To this aim, the simplest solution is to access the base layer from the cell front side by implementing a grid layout with top interdigitated contacts (TIC). In this work, we elaborate on the feasibility of the HBT structure for 3T perovskite/silicon tandem solar cells. We report, based on optical and drift-diffusion simulations, proof-of-concept designs with high efficiency potential, and we analyze, with the aid of circuit level simulations, the implications of a TIC grid layout in the perspective of scaling up to large areas. Our results show that the HBT architecture is a promising candidate for developing 3T perovskite/silicon tandem solar cells compatible with industry standard silicon photovoltaics.

**Index Terms**—perovskite-silicon tandem solar cell, three-terminal, power loss, physics-based simulation, circuit-level simulation.

## I. INTRODUCTION

Perovskite/silicon (PVS) tandem solar cells are among the most promising candidates for next generation photovoltaics [1]. They recently achieved the efficiency record of 32.5% [2], approaching that one of costly III-V double-junction solar cells [2]. Besides two- and four-terminal approaches, three-terminal (3T) tandems based on interdigitated back contact (IBC) silicon cells are currently being investigated [3], in view of the advantages of the 3T approach in terms of energy yield in the field [4].

The 3T-HBT solar cell [5], [6] offers an attractive alternative for the development of 3T PVS tandem solar cells suitable for integration with industry standard photovoltaic technologies such as PERC and heterojunction (HTJ) silicon cells. The 3T-HBT solar cell has a theoretical (material-based) efficiency limit as high as that one of a perfectly matched 2-terminal tandem, but with a simpler structure because the top and bottom subcells are seamlessly connected, without the need of any additional interconnecting layer. However, in the perspective of large-area devices, the drawback might come from the realization of the third terminal at the base layer. In fact, implementing the 3T-HBT in the PERC or HTJ silicon plat-

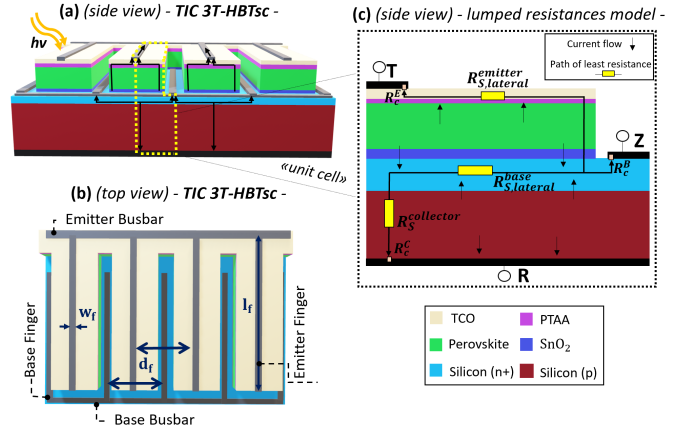


Fig. 1. TIC configuration of the 3T-HBT PVS tandem: side view (a), top view (b), side view with lumped resistance model (c).

forms requires, as simplest possible solution, adopting a top-interdigitated-contact (TIC) [7], whose implications in terms of shading and resistive losses must be carefully evaluated.

In this work, we report a simulation study of 3T-HBT PVS tandem solar cells aimed at investigating their efficiency potential and perspectives for scaling up to large areas. We present proof-of-concept 3T-HBT PVS devices designed by means of optical and transport simulations and analyze the power losses induced by the current collecting grid and how they scale with the cell area based on circuit-level simulations.

## II. DEVICE & METHODS

Fig. 1(a) sketches a 3T-HBT PVS tandem made of a  $n$ - $i$ - $p$  PVK subcell on top of a planar homojunction  $n^+$ / $p$  Si bottom cell with design parameters in line with [1]. From the top, the TCO (34 nm)/ PTAA (11 nm) / PVK(480 nm) layer stack constitutes the  $p$ -emitter layer; the  $\text{SnO}_2$  (25 nm) electron transport layer (ETL) and  $n$ -Si (150 nm) one form the base layer on top of the  $150\mu\text{m}$  thick  $p$ -type  $c$ -Si collector. The cell uses a 92 nm thick MgF antireflection coating. As shown in Fig. 1(b,c), emitter and base are accessed from the top with a TIC layout, with the base contact (Z) placed on the  $n$ -Si layer and the emitter contact (T) on the TCO layer. A full-area contact (R) is used at the collector.

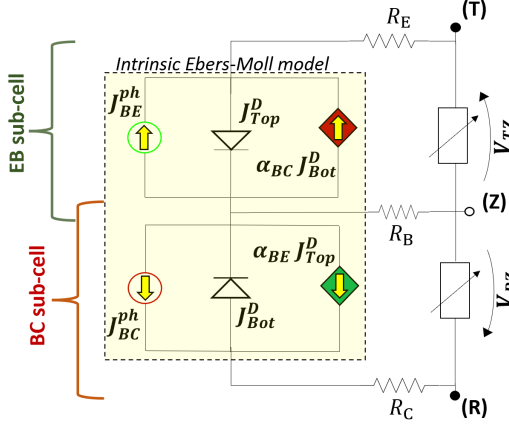


Fig. 2. Equivalent circuit of the 3T-HBT tandem.

Under illumination, photogenerated electrons and holes induce current flows collected at the T, Z and R terminals. As depicted in Fig. 1, carrier transport through materials with finite conductivity and contacts cause power loss mechanisms that can be modeled as resistive effects. The resulting equivalent circuit model of the 3T-HBT is shown in Fig. 2. It consists of the Ebers-Moll circuit of the *intrinsic* device under illumination [5], [8] completed by parasitic series resistances at each terminal. In particular, as summarized in Table I, the equivalent base and emitter series resistance account for the contribution of lateral current flow ( $R_{S,lateral}$ ) and of contact ( $R_c$ ) and finger ( $R_{finger}$ ) resistance of the current collecting grids. These are calculated based on the equivalent lumped circuit model of the unit cell of the metal grid (Fig. 1) according to the expressions given in Table I [7], [9]. At this stage, the analysis does not include the busbars.

The parameters of the Ebers-Moll model are extracted by fitting the current-voltage characteristics of the *intrinsic* 3T-HBT obtained by quasi-1D coupled optical-electrical simulations (which do not account for lateral transport neither for grid shading and resistive loss). Here, the photogeneration profile is computed by using the transfer matrix method and then given as input to the classical Poisson-drift-diffusion transport model. The approach was validated against experimental data in previous works [8], [10], where all the simulation material

TABLE I  
EXPRESSIONS OF PARASITIC RESISTANCES

Resistive loss	Label	Expression [ $\Omega \text{ cm}^2$ ]
Lateral conduction	$R_{S,lateral}$	$\frac{1}{12} R_{sh} d_f^2$
Contact	$R_c$	$\frac{1}{2} d_f \sqrt{\frac{R_{sh}}{\rho_c}} \coth\left(\frac{w_f}{2} \sqrt{\frac{R_{sh}}{\rho_c}}\right)$
Fingers	$R_f$	$\frac{1}{3} \frac{\rho_m}{t_f w_f} l_f^2 d_f$
Emitter	$R_E$	$R_{S,lateral}^E + R_c^E + R_f^E$
Base	$R_B$	$R_{S,lateral}^B + R_c^B + R_f^B$
Collector	$R_C$	$\rho_{p-Si} t_{collector}$

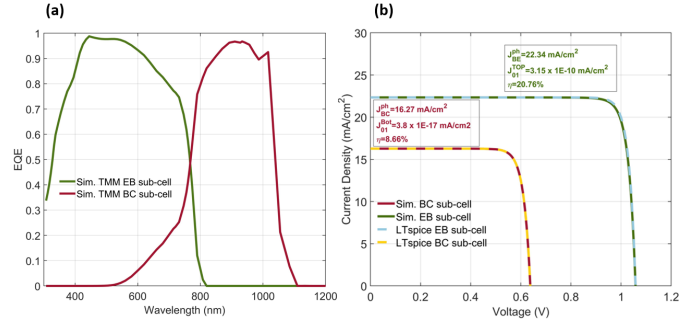


Fig. 3. (a) External Quantum Efficiency and (b)  $J$ - $V$  characteristics obtained from TCAD simulations (solid lines) and Ebers-Moll circuit fit (dashed lines).

parameters assumed are available.

### III. RESULTS & DISCUSSION

Fig. 3 shows the External Quantum Efficiency and  $J$ - $V$  characteristics of the subcells of the 3T-HBT PVS tandem under study, and the  $J$ - $V$  characteristics reproduced by the Ebers-Moll model. Transport simulations showed that band discontinuities and materials resistivity are such that the two subcells substantially work as independent, *i.e.* no appreciable transistor effect occurs through the  $\text{SnO}_2/n^+$ -Si base [8]. The *intrinsic* device has high efficiency of  $\approx 29.4\%$ .

In order to analyze the influence of the TIC grid on the device performance and scalability to large areas, we consider typical metal grid parameters [9], [11] as summarized in Table II. A shading loss factor of  $2w_f/d_f$  is applied to the bottom sub-cell, and  $3w_f/d_f$  to the top one, assuming for the etched region, needed to access the base layer, a width twice that of the metal finger.

First, we consider relatively small devices ( $l_f = 1.5 \text{ cm}$ ), in which resistive effects are dominated by lateral transport, and study the efficiency loss in terms of finger spacing and sheet resistance of the base layer, with fixed ITO/TCO emitter sheet resistance ( $\approx 274 \Omega/\square$ ). The HBT base region is composed of the bottom layer of the PVK subcell and the top layer of the Si one, therefore its sheet resistance is strongly dependent on the HBT configuration ( $p$ - $n$ - $p$  or  $n$ - $p$ - $n$ ) and bottom cell technology. As seen in Fig. 4, for  $R_{sheet}^{base}$  up to  $100 \Omega/\square$  (representative of PVS tandems on homojunction c-Si cells as in Fig.1) the efficiency loss can be minimized to less than 3%

TABLE II  
GRID GEOMETRICAL AND MATERIAL PARAMETERS

Parameter	Label	Value
Finger width ( $\mu\text{m}$ )	$w_f$	40
Finger height ( $\mu\text{m}$ )	$t_f$	15
Contact resistivity (Ag/ITO) ( $\text{m}\Omega \text{ cm}^2$ )	$\rho_c$	1.27
Contact resistivity (Ag/Si) ( $\text{m}\Omega \text{ cm}^2$ )	$\rho_c$	1
Gridline resistivity ( $\Omega \text{ cm}$ )	$\rho_m$	$2.65 \times 10^{-6}$
ITO resistivity ( $\Omega \text{ cm}$ )	$\rho_{ITO}$	$9.31 \times 10^{-4}$
c-Si( $n^+$ ) resistivity ( $\Omega \text{ cm}$ )	$\rho_{Si}$	$1.11 \times 10^{-3}$
$\text{SnO}_2$ resistivity ( $\Omega \text{ cm}$ )	$\rho_{\text{SnO}_2}$	$5.2 \times 10^{-3}$

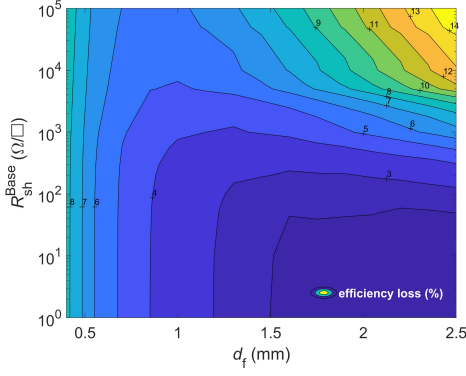


Fig. 4. Efficiency loss as a function of the finger distance ( $d_f$ ) and base sheet resistance ( $R_{sh}^{Base}$ ).

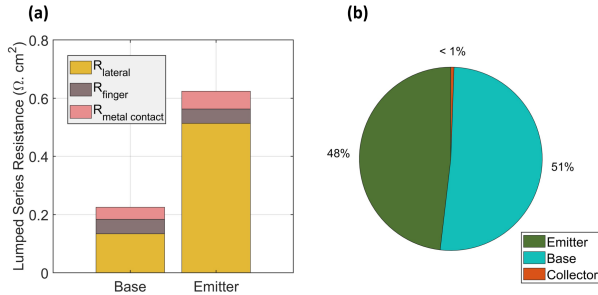


Fig. 5. (a) Emitter and base resistance components for a PVS 3T-HBT tandem with 1.5 cm x 1.5 cm area and (b) associated fractional resistive power loss.

with finger distance of 1.5 mm or larger. On the other hand, for PVS 3T-HBT tandems on HTJ silicon cells, the high sheet resistance of the a-Si:H layers ( $\approx 10^5 \Omega/\text{sq}$ ) must be mitigated by exploiting a highly conductive transport layer for the PVK top cell, such as the  $\text{SnO}_2$  layer used in the  $p$ - $n$ - $p$  HBT under study (sheet resistance  $\approx 10^3 \Omega/\square$ ).

Fig. 5 shows the emitter and base resistance and the corresponding fractional power loss estimated for the 3T-HBT PVS in Fig.1 with  $R_{sh}^{Base} = 74 \Omega/\square$ , finger length 1.5 cm, finger distance 1.5 mm. Here, the dominant resistive path is associated to the lateral transport across base and emitter. The total base resistance is about 1/3 of the emitter one, but the fractional power loss ( $\propto R J^2$ ) associated to base and emitter grids is comparable since the current through the base, which corresponds to the sum of the top and bottom subcell currents, is about 70% higher than that one of the emitter. Therefore, as the cell area and finger length increase, the resistive effects of the base grid become the dominant cause of efficiency loss.

In Fig. 6 we analyze the variation of efficiency loss with scaling up of the finger length for two values of the base sheet resistance, representative of 3T-HBT tandems on homojunction and heterojunction silicon cells. An optimized interdigitated front grid can keep power losses below 5% for finger lengths up to about 6-8 cm depending on the base sheet resistance. Such power loss could be reduced by material and device optimization, and by developing more advanced

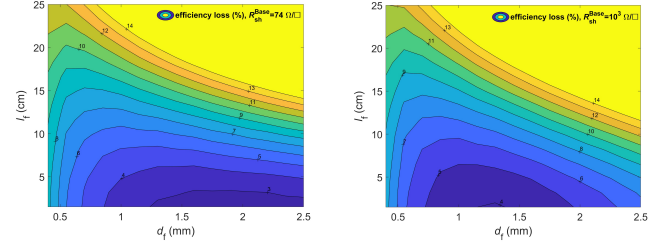


Fig. 6. Efficiency loss as a function of finger spacing ( $d_f$ ) and finger length ( $l_f$ ) for the case studies of PVS 3T/HBT on (a) homojunction Si cell ( $R_{sh}^{Base} = 74 \Omega/\square$ ) and (b) HTJ Si cell ( $R_{sh}^{Base} = 1000 \Omega/\square$ ).

grid designs, for example employing overlapped contact grids to reduce shading losses. Overall, these results show the potential, even in the perspective of scaling up to large areas, of using the HBT architecture to develop high efficiency three-terminal perovskite/silicon tandems that can be integrated with industry standard silicon bottom cells.

#### IV. ACKNOWLEDGEMENTS

This research was partly funded by the ECSEL Joint Undertaking (JU) under grant agreement No 101007247.

#### REFERENCES

- [1] C. Messmer, B. S. Goraya, S. Nold, P. S. Schulze, V. Sittinger, J. Schön, J. C. Goldschmidt, M. Bivour, S. W. Glunz, and M. Hermle, "The race for the best silicon bottom cell: Efficiency and cost evaluation of perovskite-silicon tandem solar cells," *Progress in Photovoltaics: Research and Applications*, vol. 29, no. 7, pp. 744–759, 2021.
- [2] NREL, "Best research-cell efficiencies: Emerging photovoltaics," <https://www.nrel.gov/pv/assets/pdfs/cell-pv-eff-emergingpv.pdf>, 2022.
- [3] P. Tockhorn, P. Wagner, L. Kegelman, J.-C. Stang, M. Mews, S. Albrecht, and L. Korte, "Three-terminal perovskite/silicon tandem solar cells with top and interdigitated rear contacts," *ACS Applied Energy Materials*, vol. 3, no. 2, pp. 1381–1392, 2020.
- [4] F. Gota, M. Langenhorst, R. Schmager, J. Lehr, and U. W. Paetzold, "Energy yield advantages of three-terminal perovskite-silicon tandem photovoltaics," *Joule*, vol. 4, no. 11, pp. 2387–2403, 2020.
- [5] A. Martí and A. Luque, "Three-terminal heterojunction bipolar transistor solar cell for high-efficiency photovoltaic conversion," *Nature communications*, vol. 6, no. 1, pp. 1–6, 2015.
- [6] E. Antolín, M. H. Zehender, S. A. Svatek, M. A. Steiner, M. Martínez, I. García, P. García-Linares, E. L. Warren, A. C. Tamboli, and A. Martí, "Progress in three-terminal heterojunction bipolar transistor solar cells," *Progress in Photovoltaics: Research and Applications*, vol. 30, no. 8, pp. 843–850, 2022.
- [7] M. H. Zehender, "Three-terminal heterojunction bipolar transistor solar cells = células solares de tres terminales tipo transistor bipolar de heterounión," PhD Thesis, Universidad Politécnica de Madrid, April 2022. [Online]. Available: <https://oa.upm.es/70526/>
- [8] G. Giliberti, F. Di Giacomo, and F. Cappelluti, "Three terminal perovskite/silicon solar cell with bipolar transistor architecture," *Energies*, vol. 15, no. 21, 2022.
- [9] L. Basset, "Contact electrodes for heterojunction silicon solar cells: Evaluations and optimizations of the electron contact," PhD Thesis, Université de Lille, Nov. 2020. [Online]. Available: <https://theses.hal.science/tel-03159905>
- [10] G. Giliberti and F. Cappelluti, "Physical simulation of perovskite/silicon three-terminal tandems based on bipolar transistor structure," in *Physics, Simulation, and Photonic Engineering of Photovoltaic Devices XI*, A. Freundlich, S. Collin, and K. Hinzer, Eds., vol. 11996, International Society for Optics and Photonics. SPIE, 2022, p. 1199602.
- [11] A. u. Rehman, E. P. Van Kerschaver, E. Aydin, W. Raja, T. G. Allen, and S. De Wolf, "Electrode metallization for scaled perovskite/silicon tandem solar cells: Challenges and opportunities," *Progress in Photovoltaics: Research and Applications*, 2021.